THE JOURNAL OF PHYSICAL CHEMISTRY C

Article

pubs.acs.org/JPCC

Dynamic Effects on the Charge Transport in an Organic Near-Infrared Absorber Material

K. Sebastian Radke,[†,‡] Reinhard Scholz,[§] Frank Ortmann,*[,†,‡] Karl Leo,[§,⊥] and Gianaurelio Cuniberti[†,‡,⊥]

[†]Institute for Materials Science and Max Bergmann Center of Biomaterials, Technische Universität Dresden, 01062 Dresden, Germany

[‡]Dresden Center for Computational Materials Science, Technische Universität Dresden, 01062 Dresden, Germany

[§]Institut für Angewandte Photophysik, Technische Universität Dresden, 01062 Dresden, Germany

[⊥]Center for Advancing Electronics Dresden, Technische Universität Dresden, 01062 Dresden, Germany

Supporting Information

ABSTRACT: In a theoretical study, combining molecular dynamics simulations, quantum-chemical calculations, and charge migration simulations based on Marcus theory, we investigate the electronic structure, its fluctuations, and the charge transport of a promising organic near-infrared absorber material: 7,7-difluoro-7*H*-5,9-diphenyldiisoindolo[2,1-*c*:1′,2′-*f*][1,3,5,2]triazaborinine-6-ium-7-uide (Ph_2-benz-BODIPY), which is already successfully used as the donor material in organic solar cells. For the crystalline, defect-free phase, we find a one-dimensional hole transport characteristic with a mobility of 0.53 $cm^2/(V\,s)$ and a two-dimensional electron transport characteristic with a smaller mobility of 0.15 $cm^2/(V\,s)$. The attachment of the phenyl rings to the molecular core tends to improve the electron conduction by reducing the internal reorganization energy and by increasing the intermolecular coupling. In contrast, such functionalization tends to impair the hole transport as the highest occupied molecular orbital couples dominantly to the dynamics of the phenyl rings and the annulated benzene rings.

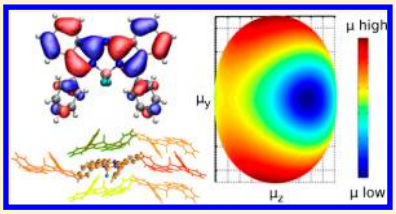

1. INTRODUCTION

Organic solar cells (OSCs) based on small molecules are potential candidates for low-cost large-area photovoltaic applications since they can be produced on flexible substrates, with little material consumption and at low temperatures.[1−3] In the past few years, especially OSCs consisting of complementary absorber materials, e.g., tandem OSCs, have gained importance in the field of organic electronics.[4] In order to improve the efficiency of these technologies, the entire sun light spectrum has to be covered by a set of different organic absorber materials. However, efficient infrared absorbers for application in OSCs are still rare and display several problematic features.[5]

The 4,4′-difluoro-4-bora-3*a*,4*a*-diaza-*s*-indacene (BODIPY) and especially the 4,4′-difluoro-4-bora-3*a*,4*a*,8-triaza-*s*-indacene (aza-BODIPY)[6] derivatives, as depicted in Figure 1A, show promising characteristics as they exhibit an absorption maximum in the near-infrared (NIR) despite their rather small π-conjugated system[7−10] as well as an enhanced thermal stability caused by the robust molecular core.[6] Additionally, functional groups can be easily included due to a convenient synthesis procedure.[9,10] For example, benzannulated aza-BODIPYs, displaying a bathochromic shift of the absorption maximum with respect to the nonbenzannulated aza-BODIPYs, are already accessible by adding aryl Grignards to phthalodinitrile followed by an in situ reduction-condensation procedure with formamide.[10,11] BODIPY derivatives find successful application in Grätzel type solar cells, showing an efficiency of up to 1.7%,[12] and as the donor material in combination with PCBM as the acceptor material in solution-processed OSCs with an efficiency of up to 2.0%.[13,14]

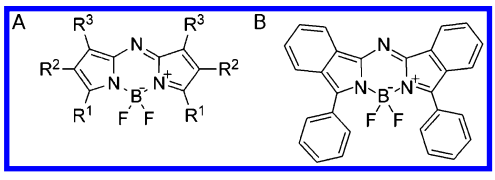

Figure 1. Molecular structure of aza-BODIPY (A) and Ph_2-benz-BODIPY (B).

In our research, we choose Ph_2-benz-BODIPY, which is known to have a relatively simple molecular structure (Figure 1B) and crystal morphology (Figure 2) compared to other members of the aza-BODIPY family and exhibits beneficial optical properties with an absorption maximum at 715 nm in solution and with a corresponding extinction coefficient of 106,000 L/mol cm.[10] In the condensed phase, the absorption maximum is shifted to 773 nm and the area of high absorption is extended up to 860 nm due to an increased π-conjugation of the molecular core compared to other aza-BODIPYs.[5] Semi-transparent OSCs incorporating a bulk heterojunction based on

Received: August 27, 2013
Revised: February 24, 2014
Published: March 6, 2014

   dx.doi.org/10.1021/jp408574d | *J. Phys. Chem. C* 2014, 118, 6537−6547

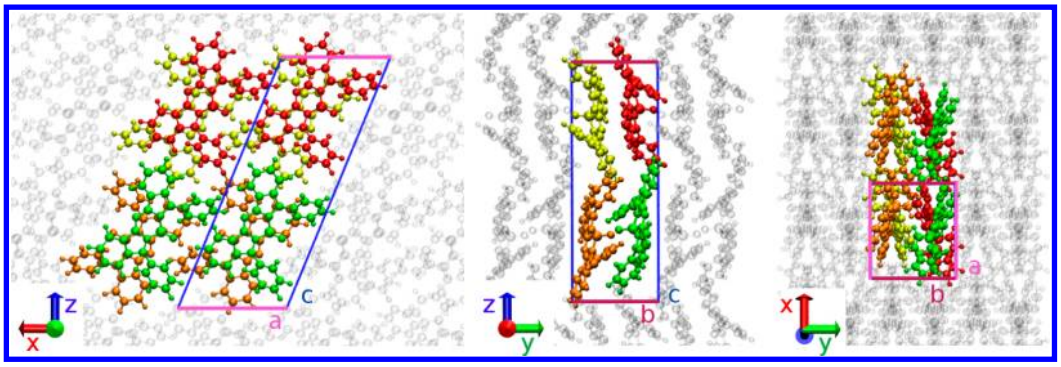

Figure 2. A 2 × 1 × 1 supercell of Ph_2-benz-BODIPY constructed according to a monoclinic unit cell (CCDC 691385/ref 11, a = 10.221 Å, b = 8.486 Å, c = 25.565 Å, β = 112.185°) along the crystal directions. The supercell contains 8 molecules. Identical basis molecules in different unit cells are depicted in the same color.

Ph_2-benz-BODIPY as the donor material and C_{60} as the acceptor are delivering efficiencies of 2.2% to 2.5%.[15]

In order to improve its performance as donor material in OSCs, relatively high hole mobilities are desirable. However, basic questions are still subject of intense debate, including the impact of the molecular structure and the supramolecular morphology on the charge transport properties. We address these topics in a theoretical study by investigating the dependence of the charge carrier mobility μ and its anisotropy for Ph_2-benz-BODIPY at 300 K on different factors:

(1) The *intramolecular* structure which determines the molecular orbitals and the intramolecular dynamics causing local energetic disorder and influencing the Huang−Rhys factors and accordingly the reorganization energies.
(2) The system morphology and the *intermolecular* packing which determine the band structure and correspondingly the transfer integrals (TIs) as well as the intermolecular dynamics causing nonlocal energetic disorder.

The main aim of this study is to understand the impact of energetic disorder effects on the charge transport characteristics in Ph_2-benz-BODIPY systems. The simulation of charge carrier transport at ambient conditions is rather complicated, as charge transport occurs via a sensitive interplay of coherent band transport and thermally activated hopping.[16,17] In systems composed of small organic molecules, the underlying charge transport mechanism strongly depends on the degree of energetic disorder. Thermal fluctuations of the orbital energies, i.e., the local energetic disorder, as well as of the TIs, i.e. the nonlocal energetic disorder, tend to localize the charge carrier over very few molecular sites.[18−21] In case of a weak electronic coupling and high temperature, the charge hopping rates between neighboring molecules can be evaluated by using semiclassical Marcus theory.[22−25] The applicability of this approach for highly ordered Ph_2-benz-BODIPY systems at 300 K will be discussed in detail in the present work.

The knowledge about the charge transport characteristics in Ph_2-benz-BODIPY gained by our studies helps in the formulation of first design rules for the class of BODIPYs and in the production of more efficient OSCs based on this class of molecules.

2. METHODOLOGY

We apply density functional theory (DFT) based methods for the evaluation of the charge transport characteristics. The computational procedure can be divided into the following steps: molecular dynamics (MD) simulation of a supercell with periodic boundary conditions, dynamic calculation of the electronic structure, which is the so-called parametrization step, and the investigation of the diffusive charge carrier mobility by means of kinetic Monte Carlo (KMC) simulations in combination with semiclassical Marcus theory. Each of these ingredients has been used to study organic materials and a combination of such methods has been employed to study transport properties in a variety of systems showing overall good agreement with experimental data. The major difference and novelty in our method is a statistical treatment of the thermal fluctuations of the orbital energies that go beyond the effect included in the internal reorganization energy as introduced in this section.

The starting point of the MD simulation is a supercell geometry taken from X-ray diffraction experiments, as depicted in Figure 2. We have chosen the smallest supercell large enough to include all possible pairs of closest neighbors existing in the crystal structure of Ph_2-benz-BODIPY (see further discussion in the Supporting Information). The Ph_2-benz-BODIPY molecule has two isomers: one with a C_2 point group while a second has a C_S point group. This publication addresses charge transport for the C_2 isomer as its crystal structure is available from X-ray diffraction experiments. Complementary investigations of the C_S isomer in the gas phase reveal no significant deviations from the C_2 isomer. The MD simulation of this system is performed at a temperature of 300 K by using the Quickstep program implemented in CP2K[26,27] which is a DFT based Born−Oppenheimer MD tool. This code is used in combination with the GTH-PADE[28−30] exchange-correlation functional and the TZV2P-GTH[31] basis set.

For the parametrization step of the electronic structure, the electronic Hamiltonian is represented in a molecular orbital (MO) basis. Correspondingly, the electronic structure of the system is described by the orbital energies ε_i at site i and the TIs ε_{ij} $(i \neq j)$, related to the coupling between orbitals on different molecules. These parameters are determined for every 0.5 fs along the MD trajectory of the molecular system by means of DFT calculations performed with the B3LYP[32−34] hybrid functional and the 6-311G[35] basis set using GAUSSIAN03.[36] In this publication, we focus on the thermal fluctuations of the electronic structure and their impact on charge transport characteristics. The orbital energies and the TIs are obtained by performing monomer and dimer calculations, respectively. Electrostatic contributions are neglected,[24,37] but an estimation for the impact of these

dx.doi.org/10.1021/jp408574d | J. Phys. Chem. C 2014, 118, 6537−6547

contributions on the charge carrier mobility is discussed in the Supporting Information.

The charge carrier mobility μ is obtained by simulating stochastically the propagation of a single charge carrier by means of KMC simulations. The charge transfer rates are evaluated by using a standard form of semiclassical Marcus theory

$$k_{ij} = \frac{\varepsilon_{ij}^2}{\hbar}\sqrt{\frac{\pi}{\lambda k_B T}}\ \exp\left[-\frac{(\Delta G_{ij} - \lambda)^2}{4k_B T\lambda}\right] \quad (1)$$

where λ is the total reorganization energy of a molecule, k_B is the Boltzmann constant, T is the temperature (300 K for all simulations), and ΔG_{ij} is the free energy difference of the initial and the final molecular states.[22−25] λ can be divided in two different contributions being the inner-sphere part λ_i which is related to the structural changes of the reacting molecule and the outer-sphere part λ_o which is caused by the relaxation of the surrounding solvent. In this work, we neglect any environmental relaxation as well as changes in the electronic polarization, and describe the total reorganization energy λ only by its intramolecular contributions λ_i. This quantity can be accessed from the adiabatic potential energy surfaces for the neutral and ionic states by DFT calculations (Gaussian03, B3LYP/6-311G(d,p)) according to[22,38]

$$\lambda_{\pm} = \lambda_{rel}^{(1)} + \lambda_{rel}^{(2)} \quad (2)$$

$$\lambda_{\pm} = [E_0(\pm) - E_0(0)] + [E_{\pm}(0) - E_{\pm}(\pm)] \quad (3)$$

Hereby, $\lambda_{rel}^{(1)}$ denotes the relaxation energy for the neutral molecule with $E_0(\pm)$ the energy of the neutral molecule in the equilibrium geometry of the ionic state and $E_0(0)$ the equilibrium energy of the neutral molecule. $\lambda_{rel}^{(2)}$ is the relaxation energy for the molecule in the ionic state with $E_{\pm}(0)$ the energy of the ionic molecule in the equilibrium geometry of the neutral state and $E_{\pm}(\pm)$ the equilibrium energy of the molecule in the ionic state.

To investigate the contribution of each vibrational mode to the relaxation processes, the normal mode approach is applied for a calculation of the relaxation energy of the neutral molecule $\lambda_{rel}^{(1)}$.[38,39] It is based on a power series expansion of the potential energy of the neutral state in the normal mode coordinates

$$\lambda_{rel} = \sum_j \lambda_j = \sum_j \frac{k_j}{2}(\Delta Q_j)^2 = \sum_j S_j \hbar\omega_j \quad (4)$$

where λ_j denotes the contribution of mode j to the relaxation energy, k_j the respective force constant, ΔQ_j the displacement along the mode j, $\hbar\omega_j$ the vibrational energy, and S_j the Huang−Rhys factor. For a calculation of the contributions λ_j for hole (electron) transfer, the deformation of the molecular structure upon charging the neutral molecule toward the relaxed cationic (anionic) state is determined and projected onto the complete set of vibrational eigenvectors of the neutral molecule. All calculations are performed at a DFT level of theory (Gaussian03, B3LYP/6-311G(d,p)[35]). Consequently, we apply a scaling factor of 0.967 for the frequencies of the vibrational modes $\hbar\omega_j$, but we conserve the relaxation energies λ_j by increasing the Huang−Rhys factors S_j by a factor of 1/0.967.[40]

The free energy difference is described by the difference in the orbital energies

$$\Delta G_{ij} = \varepsilon_i - \varepsilon_j \quad (5)$$

which is subject to thermal fluctuations of the orbital energies ε_i. Such fluctuations of frontier MO energies can be described by a Gaussian density of states (DOS) with standard deviation σ (see Figure S1, Supporting Information, for details). As all normal modes contribute to the MD trajectories and therefore also to the standard deviation of the orbital energies, the latter contains contributions of the modes that are already included in the internal reorganization energy λ. Thus, for a correct definition of ΔG_{ij} and of the diabatic states, we only include the impact of anharmonic effects and crystal field effects on the thermal fluctuations of the orbital energies that are not covered by the internal reorganization energy λ by using

$$\sigma_{dyn}^{\ 2} = \sigma_{anharm}^{\ 2} + \sigma_{crystal}^{\ 2} \quad (6)$$

To deduce crystal field effects, the time series of the frontier MOs of a molecule in the gas phase and a molecule in the condensed phase are analyzed statistically to obtain the standard deviations σ_{MD}^{gas} and σ_{MD}^{cond}, respectively. As σ_{MD}^{cond} includes the influence of the crystal field on the fluctuations of the frontier MO energies, whereas σ_{MD}^{gas} does not, we can calculate the standard deviation $\sigma_{crystal}$ containing only the influence of the crystal field as follows

$$\sigma_{crystal}^{\ 2} = (\sigma_{MD}^{cond})^2 - (\sigma_{MD}^{gas})^2 \quad (7)$$

The evaluation of anharmonic effects is more complex. It is clear that σ_{MD}^{gas} includes harmonic as well as anharmonic contributions to the fluctuations of the MO energies where the degree of anharmonicity depends on the occupation. We assume that at a temperature of 300 K only low frequency modes (below ω_{cutoff} = 300 cm^{-1}) are occupied in higher states than the ground state and that only these modes have anharmonic contributions.[41] Consequently, the standard deviation σ_{anharm} containing only the influence of anharmonic effects on the fluctuations of the orbital energies can be calculated by using the expression

$$\sigma_{anharm}^{\ 2} = [\sigma_{MD}^{gas}(\omega < \omega_{cutoff})]^2 - [\sigma_{harm}(\omega < \omega_{cutoff})]^2 \quad (8)$$

As these modes can be treated classically ($k_B T \gtrsim \hbar\omega_j$), the standard deviation of the orbital energies in the harmonic approximation is given as[42−44]

$$\sigma_{harm}^{\ 2}(\omega < \omega_{cutoff}) = \sum_{\omega_j < \omega_{cutoff}} 2\lambda_j k_B T \quad (9)$$

For the propagation, a semi-infinite three-dimensional molecular lattice is built according to the relaxed crystal structure since we are interested in the intrinsic charge carrier mobility in highly ordered Ph_2-benz-BODIPY. Correspondingly during the KMC simulations the molecular positions are kept fixed. The electronic structure is represented statistically on the molecular lattice,[45,46] i.e. for each hopping event the orbital energies ε_j of each neighboring molecule j are taken at random following a Gaussian distribution according to σ_{dyn}. The TIs are kept fixed during the charge propagation as it was found that the correlation time is much smaller compared to the average hopping time.[47] Consequently, in eq 1, $\varepsilon_{ij}^{\ 2}$ is represented by its time-averaged value

$$\langle \varepsilon_{ij}^{\ 2} \rangle = \langle \varepsilon_{ij} \rangle^2 + \sigma_{ij}^{\ 2} \quad (10)$$

dx.doi.org/10.1021/jp408574d | J. Phys. Chem. C 2014, 118, 6537−6547

where $\langle \varepsilon_{ij} \rangle$ is the average value of the TI and σ_{ij} is the corresponding standard deviation. Both values are obtained from the time series of the TIs.

3. ELECTRONIC SYSTEM PARAMETERS

The charge transfer rate k_{ij} and, thus, the charge carrier mobility μ are influenced by three parameters in eqs 1,5,10:

(1) the reorganization energy λ,
(2) the thermal fluctuation σ of the orbital energy ε_i determining the local energetic disorder,
(3) the average absolute values of the TIs ε_{ij} as well as their thermal fluctuations determining the width σ_{ij} of nonlocal energetic disorder.

A detailed investigation of the intramolecular electronic structure of the Ph_2-benz-BODIPY molecule and accordingly an analysis of the first two parameters are given in section 3.1, while section 3.2 addresses the intermolecular electronic properties, i.e., the band structure and the TIs. Section 4 presents the results of the charge transport simulations.

3.1. Local Electronic Structure Properties. For a single Ph_2-benz-BODIPY molecule of the relaxed supercell, the HOMO energy equals −5.25 eV and is well separated from the HOMO-1 at −7.17 eV. Similarly, the LUMO energy at −3.21 eV is well below the LUMO+1 energy at −1.38 eV. Consequently, as a first important result, we can state that only the frontier MOs play a significant role in the conduction process, i.e. the HOMO for hole transport and the LUMO for electron transport. In the following, we will focus only on their energies and on the respective TIs.

Structural Analysis of the Frontier Orbitals. The frontier orbitals are displayed in Figure 3. Interestingly, we find that the

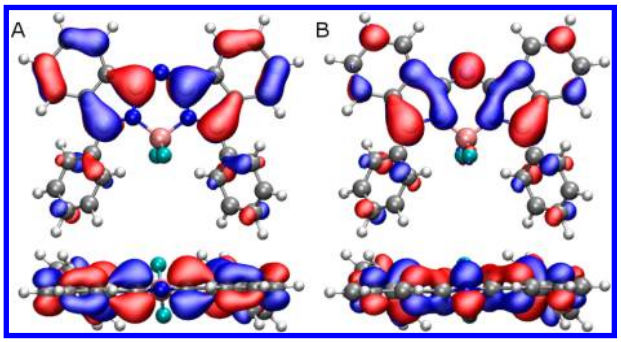

Figure 3. HOMO (A) and LUMO (B) of Ph_2-benz-BODIPY (front and top views).

HOMO and the LUMO are delocalized over the whole molecule which potentially leads to a strong intermolecular coupling and improves the charge transport especially in amorphous materials as has been reported for BTDF.[48] This strong delocalization is also in analogy to the orbital structures of popular molecules investigated in the context of OSCs, such as rubrene, where the contributions to the orbitals at the attached phenyl rings are relatively low, but significantly improve the TIs.[49,50]

The structures of the HOMO and the LUMO differ mainly at the molecular core. The dominant contribution to the LUMO, which is mirror-symmetric with respect to a vertical plane, is made by atoms located at the central ring including the N−B−N-group. In contrast, the coefficients of the HOMO vanish at the nitrogen atoms contained in the vertical N−B−N plane because of the odd symmetry of the HOMO with respect to this plane. Additionally, the HOMO extends more over the annulated benzene rings compared to the LUMO.

Deformation Patterns for Charged Molecules. Figure 4 shows the deformation of the molecular structure upon

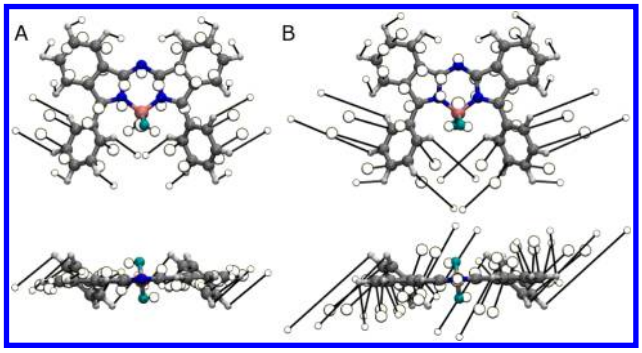

Figure 4. Deformation in the cationic (A) and anionic (B) geometry of Ph_2-benz-BODIPY (open spheres) with respect to the geometry in the electronic ground state (front and top views). For reasons of visibility, the deformation is increased by a factor of 20.

charging the neutral molecule toward the relaxed cationic and anionic state. The strongest deformations are observed at the substituents (phenyl rings at the 3,5-position), which are rotated toward a smaller torsional angle with respect to the molecular plane (Figure 4 lower panels) and shifted away from the symmetry axis (Figure 4 upper panels). These deformations are stronger for the anionic state than for the cationic state. Moreover, strong deformations can also be seen at the annulated benzene rings. For both the cationic and the anionic deformation, the annulated rings are rotated in-plane around the center of mass resulting in a shift toward the symmetry axis (Figure 4 upper panels). The atoms of the annulated rings are also moved slightly out-of-plane in the anionic state (Figure 4B lower panel). In contrast, these atoms are shifted predominantly in-plane for the cationic deformation as shown in the lower panel of Figure 4A.

Although the torsional deformations at the phenyl rings and the annulated benzene rings show the largest structural changes for the transition from the electronic ground state toward the relaxed cationic and anionic state, they do not dominate the relaxation energetically. This is especially true in the condensed phase, when intermolecular interactions tend to disable the torsional motion of the phenyl rings at the 3,5-position. In contrast, the small shifts in the geometry of the molecular core are much more significant as will be seen in the further analysis. In general, the deformations at the central ring and the pentagons occur consistently to the structure of the frontier MOs, i.e., the HOMO for the cationic deformation and the LUMO for the anionic deformation. For the latter case, the bond lengths are decreased for bonding lobes of the MO, and for antibonding nodes the bond lengths are increased. A reverse trend is observed for the cationic deformation.

Internal Reorganization Energy and Huang−Rhys Factors. By using the potential energy surface approach and eq 3 to calculate the internal reorganization energy, we obtain $\lambda_+ = 139$ meV for hole transport and $\lambda_- = 222$ meV for electron transport. This indicates that according to eq 1 the rate k_{ij} for hole transport might be much larger than the rate for electron transport.

dx.doi.org/10.1021/jp408574d | J. Phys. Chem. C 2014, 118, 6537−6547

In order to analyze the contribution of each vibrational mode to the relaxation processes with the normal mode method, the presence of Dushinsky rotations in the deformations from the electronic ground state to the ionic states as shown in Figure 4 has to be corrected. Correspondingly we calculate the Huang–Rhys factors S_j and the relaxation energies λ_j for auxiliary ionic geometries constructed with frozen dihedral angles (see Figure S2 for information).[51] By using these deformation patterns, we obtain results in good agreement with the approach relying on the potential energy surface (see Table S1), serving as a numerical confirmation of the equivalence of both methods.

Analyzing the Huang–Rhys factors depicted in Figure 5A and given in detail in the Supporting Information in Table S2, one finds three main contributions:

(1) Low energy vibrations with frequencies up to about 500 cm^{-1} (Figure 5A, no. 1), assigned to torsional modes and out-of-plane bending modes with strong contributions of the central ring.
(2) Intermediate energy vibrations with frequencies around 1000 cm^{-1} (Figure 5A, no. 2), consisting of complex combinations of in-plane B–N, C–C, and C–H bending modes.
(3) High energy vibrations with frequencies between 1300 and 1600 cm^{-1} (Figure 5A, no. 3) dominated by in-plane C–H bending modes and C–C stretching modes.

In agreement with the observations made for the internal reorganization energy, the electrons couple more strongly to the vibrational modes than the holes, which is a result of the larger deformation of the anionic state shown in Figure 4B and Figure S2B. The structural assignments of the normal modes with the highest Huang–Rhys factors are given in the Supporting Information in Table S3. The Huang–Rhys factors for electron transfer strongly correlate with the motion of the boron atom on the central ring and, thus, dominant electron–phonon coupling elements are obtained for low energy vibrational modes and in-plane bending modes of the central ring with intermediate energy. This observation agrees with the localization of the LUMO around the central ring involving the boron atom, as shown in Figure 3B. In contrast, the size of the Huang–Rhys factors for hole transfer depends on the vibrational deformation of the annulated rings and especially at the phenyl rings (Table S3). Thus, dominant hole-phonon coupling elements are determined for low energy vibrational modes as well as high energy C–C stretching and C–H bending modes. The corresponding relaxation energies are depicted in Figure 5B.

Chemical Substitution Effect on λ. As several benzannulated aza-BODIPYs with different functional groups at the 3,5-position have been reported and show promising light absorption characteristics,[10] we want to investigate the influence of the functionalization on the reorganization energy by comparing the results obtained for Ph_2-benz-BODIPY with the ones for H_2-benz-BODIPY (Figure S3 in the Supporting Information). By substituting the phenyl rings at the 3,5-position by hydrogen atoms, this molecule represents the case of frozen side groups. Especially by regarding the deformation patterns for Ph_2-benz-BODIPY displayed in Figure 4, one would expect a clear decrease in the reorganization energy for H_2-benz-BODIPY with respect to Ph_2-benz-BODIPY. However, we obtain a surprising result: while the reorganization energy for hole transfer λ_+ decreases from 139 to 113 meV (as expected), the reorganization energy for electron transfer λ_- increases slightly from 222 to 236 meV (potential energy surface approach) when replacing the phenyl groups. This indicates that especially electron transfer can be improved due to a proper choice of the substituents (H → Ph), while hole transfer might be impaired due to the functionalization which is an undesired effect if the material is supposed to be used as the donor material in OSCs. However, the observation made for electron transfer is surprising since in investigations of the influence of functional groups on the reorganization energy, a

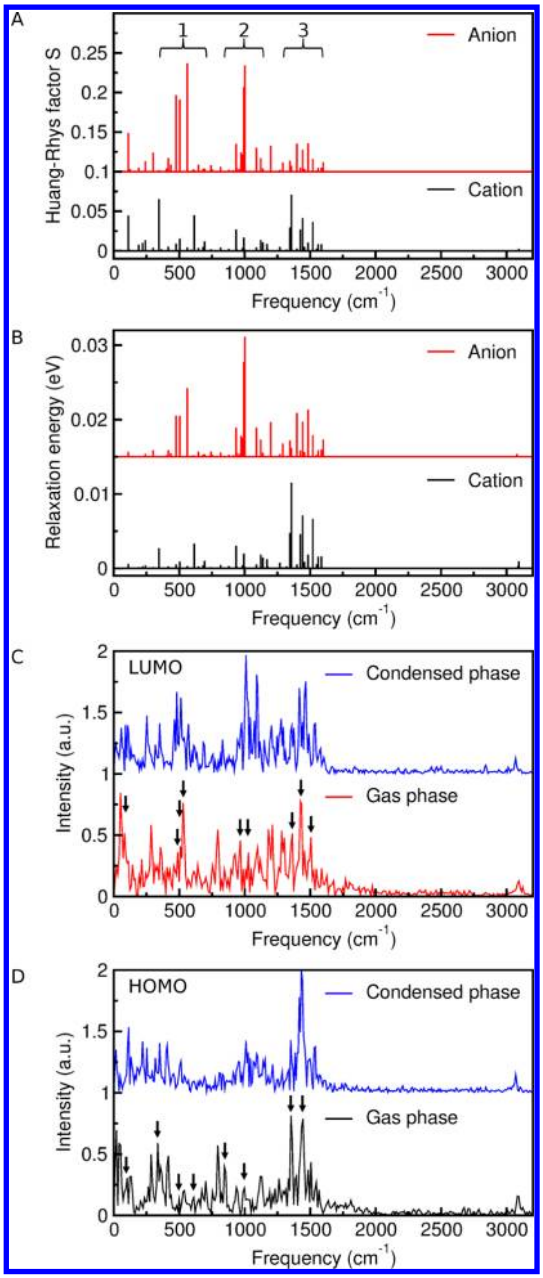

Figure 5. Huang–Rhys factors (A) and relaxation energies (B) of the electronic ground state of Ph_2-benz-BODIPY for electron (anion) and hole (cation) transfer. The Huang–Rhys factors and the relaxation energies are obtained based on auxiliary relaxed ionic geometries with frozen dihedral angles. The mode energies in panels (A) and (B) are scaled by a factor of 0.967 and the Huang–Rhys factors by 1/0.967.[40] Fourier transforms of the time series of the LUMO energy (C) and the HOMO energy (D) of a molecule in the gas and in the condensed phase. The arrows indicate normal modes with substantial Huang–Rhys factors in the gas phase (Figure 5A, Table S3).

dx.doi.org/10.1021/jp408574d | J. Phys. Chem. C 2014, 118, 6537–6547

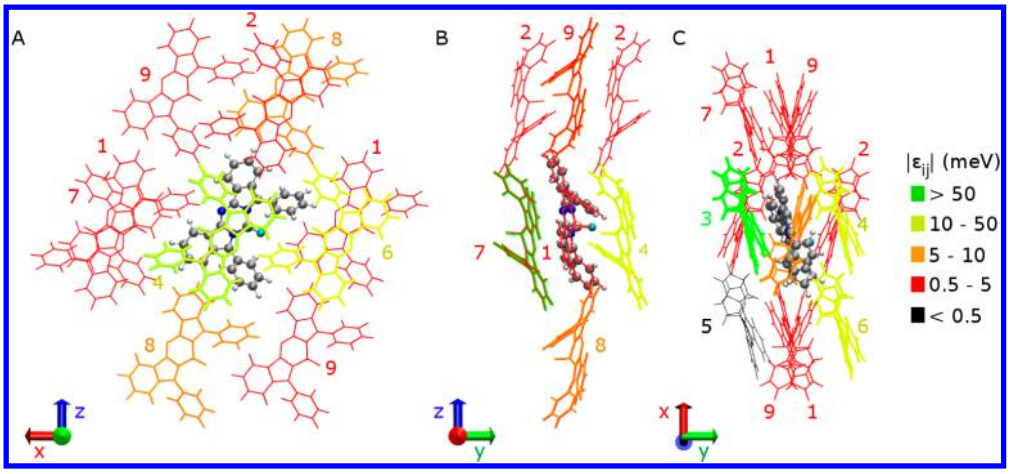

Figure 6. Illustration of the 13 closest neighbors and definition of the 9 most important TIs between HOMOs. The neighboring molecules are colored according to the size of the HOMO−HOMO TIs in the relaxed Ph_2-benz-BODIPY crystal. The numbers denote the classification of the TI as used in Table S4. The HOMO−HOMO TIs are anisotropically arranged with one dominant conduction channel (TI3 and TI4) in y direction.

trend toward an increase in the internal reorganization energy due to the attachment of substituents has been reported.[52] On the other hand, the selective tunability of the transport features of only one charge species appears as an interesting perspective on its own.

The change in the reorganization energy for hole transfer from H_2-benz-BODIPY to Ph_2-benz-BODIPY can be traced back to the contributions λ_j made by the vibrational modes at the phenyl rings. While the contribution of high energy modes remains nearly unchanged, an increase of the contributions of low and especially intermediate energy modes causes an increase of the total reorganization energy as can be seen by comparing Figure 5B with Figure S3D. To understand the decrease of the reorganization energy for electron transfer in Ph_2-benz-BODIPY, one has to compare the deformation patterns depicted in Figure 4B and in the right panel of Figure S3B. The deformation of the central ring which is mostly affecting the electron−phonon coupling elements is more pronounced for H_2-benz-BODIPY than for Ph_2-benz-BODIPY. This results in a large decrease of the contributions by high energy modes for Ph_2-benz-BODIPY, which cannot be compensated by an increase in the contributions by low and intermediate energy modes.

Dynamical Analysis of the Frontier Orbital Energies. The Fourier transforms of the time series of the MO energies obtained for a molecule in the gas phase and a molecule in the condensed phase within the simulated supercell are analyzed. This helps to gain further insight into the coupling of the frontier MOs to the dynamics of the molecule. The resulting spectra are displayed in panels C and D of Figure 5. We observe that the spectra are qualitatively in good agreement with the results discussed in the previous part, i.e. normal modes with large Huang−Rhys factors S_j and reorganization energies λ_j are also pronounced in the spectra (Figure 5, parts C and D), as indicated by the arrows.

The comparison between gas phase and condensed phase can be used to investigate the impact of the crystal field on the coupling of the MOs to the vibrational modes. For both the HOMO and the LUMO, we find a decrease for the intermolecular vibrational modes below 300 cm^{-1} and out-of-plane bending modes around 800 cm^{-1} by switching from the gas phase to the condensed phase. As these vibrational modes contribute simultaneously to both the hole-phonon coupling and the electron−phonon coupling (Figure 5A), it seems that the fluctuations of the HOMO and the LUMO are similarly affected.

Statistical Analysis of the Frontier Orbital Energies. In addition to their influence on the internal reorganization energy λ, thermal fluctuations of the frontier MO energies also contribute to the free energy difference ΔG_{ij} as explained in Sec. 2. First, we analyze the Gaussian distributions of the orbital energies ε_i without performing the discussed corrections introduced by eqs 7 and 8. In the condensed phase, we find $\varepsilon_{HOMO} = (-5.244 \pm 0.062)$ eV and $\varepsilon_{LUMO} = (-3.240 \pm 0.072)$ eV, showing a higher local energetic disorder for the LUMO with respect to the HOMO, which is in accordance with our expectations from the structural and dynamical analysis of the orbital energies. In the gas phase, we obtain $\varepsilon_{HOMO} = (-5.240 \pm 0.052)$ eV and $\varepsilon_{LUMO} = (-3.230 \pm 0.064)$ eV. Consequently, the crystal field yields an increase in the local energetic disorder in going from gas phase toward the condensed phase that is similar for both MOs. Nevertheless, this effect is surprising as one would expect that the crystal field is reducing the local energetic disorder by hindering the molecular dynamics.

When considering these fluctuations for the free energy difference ΔG_{ij} in eq 1, we have to apply a correction as discussed in the methodology part. Figure S4 shows the accumulated standard deviations, σ_{harm} (eq 9), σ_{MD}^{gas}, and σ_{MD}^{cond} as a function of a cutoff frequency ω_{cutoff}. The curves confirm the assumption formulated in section 2 that ω_{cutoff} can be set to 300 cm^{-1} at 300 K. On the basis of these data, for the HOMO and the LUMO, we obtain nearly identical values for σ_{dyn} with 33 and 30 meV, respectively. Thereby, the contributions made by anharmonicities are similar for both MOs, while the contributions by the crystal field are stronger for the HOMO.

3.2. Non-Local Electronic Structure Properties. To gain more insight into the directional dependence (anisotropy) of electronic properties, we focus in this section on the electronic coupling between neighboring molecules. From the analysis of the TIs and their fluctuations, one can investigate the preferred conduction directions in the crystalline system, the degree of nonlocal energetic disorder, and the localization of the charge carriers. Correspondingly we compare the TIs of the relaxed supercell with the statistically analyzed TIs obtained from the simulated MD trajectory at 300 K.

dx.doi.org/10.1021/jp408574d | J. Phys. Chem. C 2014, 118, 6537−6547

Basically, each molecule has 16 close neighbors with finite orbital overlap. As the charge transfer rate in eq 1 depends quadratically on the TI, we only include the TIs with $|\varepsilon_{ij}| \geq 0.5$ meV, reducing the number of closest neighbors considered in the charge transport simulations to 13. Additionally, some molecular combinations are structurally equivalent for symmetry reasons, decreasing the number of different couplings to 9 TIs as shown in Figure 6. The full set of TIs of the relaxed supercell as well as the averaged values for the system simulated at 300 K are given in Table S4 in the Supporting Information. Here, we discuss only the most important features.

In Figure 6, the closest neighbors of a given molecule are displayed and colored according to the absolute value of the HOMO−HOMO TIs of the relaxed system. These images reveal a highly anisotropic spatial distribution of the TIs with one clearly dominant TI (denoted TI3). The pair connected by TI3 has strong $\pi-\pi$ overlap because the extended molecular cores are ordered almost parallel to each other. In the relaxed system, TI3 dominates by far with an absolute value of 116 meV. On the opposite side of the central molecule, we define TI4 which exhibits an absolute HOMO−HOMO TI of 26 meV, significantly smaller than TI3. The steric hindrance arising from the phenyl rings increases the distance between the molecules, reducing the orbital overlap accordingly. Both TI3 and TI4 define a linear conduction channel along the y axis since all other TIs are significantly lower (see Table S4). From the TIs with larger molecule separation, only TI6 shows an absolute HOMO−HOMO TI that is larger than 10 meV, arising from an orbital overlap between the phenyl rings.

By comparing the HOMO−HOMO TIs of the relaxed system with the corresponding average values obtained at 300 K (Figure S5A−C), we observe a decrease in the dominance of TI3 (Table S4). Because of the vibrational motion of the phenyl rings, the high $\pi-\pi$ overlap of the molecules is disturbed, reducing the average value from 116 to 98 meV. In contrast, the average values of TI4 and TI6 remain almost unchanged, but their distributions show a higher relative standard deviation. For the molecules with low TIs in the relaxed structure, we observe an increased average value by including thermal effects.

Analogous considerations of the distribution of the LUMO−LUMO TIs in the relaxed system as well as at 300 K can be found in Figures S5D to S5I in the Supporting Information. The results for the LUMO−LUMO TIs are similar, so we briefly highlight only the main differences to the HOMO−HOMO TIs (see Table S4 for details). We observe an analogous anisotropy, but the most significant TIs (TI3, TI4, and TI6) are almost a factor of 2 smaller than the corresponding HOMO−HOMO TIs. According to eq 1, this decreases the electron transfer rate k_{ij} by a factor of about 4 with respect to the hole transfer rate. Regarding the fluctuations of the TIs, the standard deviations of TI3, TI4, and TI6 are clearly increased with respect to the corresponding standard deviations obtained for the HOMO−HOMO TIs. This can be assigned to the relatively strong coupling of the LUMO to the vibrational modes including deformations of the central ring.

Already from an analysis of the TIs, we observe that crystalline Ph_2-benz-BODIPY tends to be a quasi one-dimensional charge transport material with a dominant charge transfer along the y direction. Without including energetic disorder effects, the dimensionality of the charge carrier transport as well as the localization of the charge carriers can be investigated by analyzing the band structure of the Ph_2-benz-BODIPY crystal. The calculations are performed based on the relaxed unit cell (CP2K, GTH-PADE/GTH-TZV2P) at a DFT level of theory (VASP,[53−55] LDA[56,57]). Although LDA tends to underestimate the band gap as can be seen for the HOMO and LUMO bands in Figure 7, the widths of the bands are usually

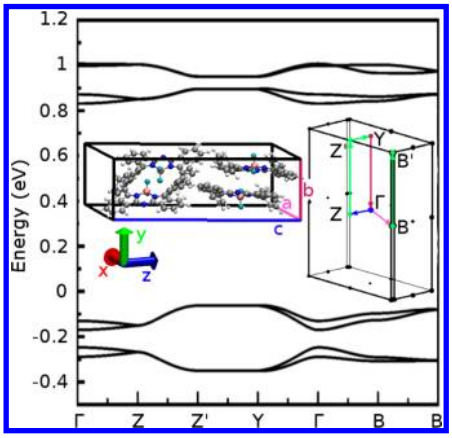

Figure 7. DFT-band structure of the Ph_2-benz-BODIPY crystal showing the HOMO and LUMO bands. The included panels depict the unit cell the definition of special points in the Brillouin zone as well as the path through the Brillouin zone. Corresponding directions are indicated by the same colors.

considered reliably.[58] The results are in good agreement with the investigations on the TIs in the Ph_2-benz-BODIPY crystal. The strongest band dispersion occurs in the ΓY direction for both the HOMO and the LUMO bands. This most dispersive direction in reciprocal space corresponds to the b direction in real space (y axis), in agreement with the high values obtained for TI3 and TI4. The band dispersion is also more pronounced for the HOMO bands than for the LUMO bands, confirming the larger HOMO−HOMO TIs compared to the LUMO−LUMO TIs. For the HOMO bands, a significant (though smaller) band dispersion can also be found in the ΓB direction arising from TI6 indicating quasi one-dimensional charge carrier transport for both electrons and holes.

4. CHARGE TRANSPORT SIMULATIONS

Electron and hole mobilities are obtained by KMC simulations as described in section 2. Thereby each single run i defines an end position $\vec{r}_i$ and the respective arrival time t_i of a charge carrier. We project $\vec{r}_i$ onto a spatial direction according to the normalized radial vector $\vec{e}(\theta,\varphi)$ and average over all KMC runs i to obtain the spatial angular dependence (spherical angles θ and φ) of the average moved distance and carrier mobility according to

$$\mu(\theta, \varphi) = \frac{1}{k_B T} \left\langle \frac{[\vec{r}_i \cdot \vec{e}(\theta, \varphi)]^2}{2t_i} \right\rangle_i \tag{11}$$

Finally, the averaged charge carrier mobility μ is determined by integrating over all directions θ and φ.

We obtain an average hole mobility μ_+ of 0.53 $cm^2/(V\,s)$ and an average electron mobility μ_- of 0.15 $cm^2/(V\,s)$. This result confirms our expectation of more facile hole transport formulated on the basis of the electronic structure. We identify two main factors for the electron−hole asymmetry: the reorganization energy for electron transfer λ_- is larger than λ_+ by more than 50% and the LUMO−LUMO TIs are smaller

dx.doi.org/10.1021/jp408574d | J. Phys. Chem. C 2014, 118, 6537−6547

than the HOMO−HOMO TIs by roughly a factor of 2. In contrast, the standard deviation of the LUMO energy caused by anharmonicities and the crystal field is nearly identical to the value obtained for the HOMO energy.

The anisotropy of the hole mobility is depicted in Figure 8A and Figure S6. The distribution of the hole mobility $\mu(\theta,\varphi)$

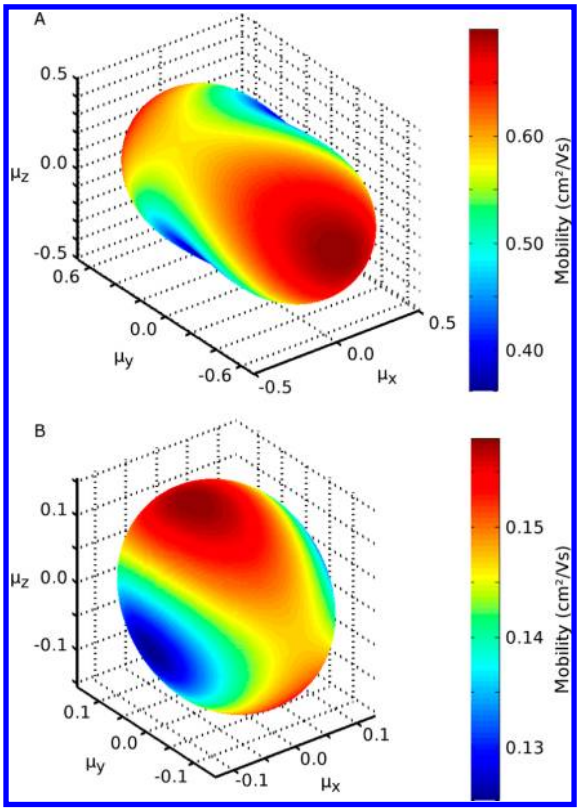

Figure 8. Distribution of the hole (A) and electron mobility (B) of Ph_2-benz-BODIPY in space.

resembles a pea-pod-like spheroid along the *y* axis (Figure 8B), where we also obtained the largest TIs (TI3, TI4). Notwithstanding, the hole mobility is surprisingly low given the strong intermolecular couplings. The reason is the asymmetric one-dimensional character of the conduction channels, where 86% of all jumps occur along TI3 (Table S5); i.e., holes move mainly forth and back between the molecules. This indicates that due to the anisotropy of the crystalline structure, the charge carrier is mostly localized on two adjacent molecules connected by the largest TI. Correspondingly we find that this large TI is not significantly contributing to the net transport. Such bottleneck effects have been reported for one-dimensional molecular systems[59] and molecular systems with static disorder.[24] We can conclude that in real devices hole transport in Ph_2-benz-BODIPY might be more susceptible to defects due to the one-dimensional character.

The anisotropy of the electron mobility is shown in Figure 8B. In contrast to holes, the simulation gives an oblate spheroid approximately oriented in the yz plane. Surprisingly, the highest electron mobilities occur roughly in z direction followed by somewhat lower values along the *y* axis. Although the highest TIs are observed in y direction, the molecule has only 2 neighbors to which the charge carrier can hop. In the other spatial directions, even though the TIs remain significantly smaller, the number of neighbors is higher, providing more pathways, which seems to be more important for a robust electron transfer. Here, 81% of all jumps occur along TI3 (Table S6), which is only slightly smaller than for holes. Nevertheless, the somewhat better availability of other transport channels reduces the anisotropy of the electron mobility significantly.

5. DISCUSSION

In this discussion, we address mainly two points. In the first part, we use our results to discuss qualitative aspects of charge transport of Ph_2-benz-BODIPY in the amorphous phase. In the second part, the applicability of the semiclassical Marcus theory for charge transport investigations in a highly ordered Ph_2-benz-BODIPY system is discussed.

5.1. Charge Transfer in the Amorphous Phase. In the solar cells using Ph_2-benz-BODIPY as the donor material, this material has formed amorphous structures.[5,15] Although the main aim of our studies is the simulation of charge transport in highly ordered Ph_2-benz-BODIPY systems, it is therefore interesting to relate our findings to the conduction in the amorphous phase. The analysis of the contributions of the normal modes to the internal reorganization energy is based on gas phase simulations that are largely valid independently from the system morphology. Here, we find that the reorganization energy is much larger for electrons than for holes. Moreover, the intermolecular coupling between the HOMOs of neighboring molecules in the crystal phase is overall higher than between the LUMOs. In the amorphous phase, where only short-range order survives, it can be expected that this trend is robust because the HOMO has stronger contributions than the LUMO both at the phenyl rings and the annulated rings, increasing the probability for a substantial orbital overlap. Consequently, we expect that in amorphous Ph_2-benz-BODIPY, the hole mobility remains larger than the electron mobility. However, due to the impact of static disorder, both mobilities should reduce significantly compared to the ones obtained for highly ordered systems.[5] Unfortunately, there is very little experimental information about the type of disorder, its strength or other characteristics available for this material class. However, in the Supporting Information, a discussion of the impact of weak static disorder following the Anderson disorder model is addressed.[60−63] Such uncorrelated disorder mimics defects and impurities as a first approximation and gives a first impression of the effect of disorder on the charge carrier mobility. Additionally, an isotropic charge transport is expected for the amorphous phase and, thus, bottleneck effects as observed in the crystal should be reduced.

5.2. Applicability of Marcus Theory. As we observed a dominant hole conduction, the following discussion is only presented for the case of hole transport, but it applies equally for electrons.

The largest HOMO−HOMO TI (TI3) shows an absolute value of 116 meV in the relaxed system. As all other TIs are significantly smaller (the second largest value is 26 meV (TI4) being much smaller than λ_+ = 139 meV), 86% of all hopping events occur between the pair of molecules (dimer) defining TI3, limiting the hole mobility significantly. This can be understood in terms of bottleneck effects which seem to be even stronger than in other one-dimensional charge transport materials.[59] Consequently, we can assume that the charge carrier is highly localized at the molecular dimers, and the reactants of the charge transfer reaction in the Marcus picture

dx.doi.org/10.1021/jp408574d | J. Phys. Chem. C 2014, 118, 6537−6547

might be better represented by these dimers. Also, the resulting average hole mobility of 0.53 $cm^2/(V\ s)$ remains far below values that have been proposed for hopping transport in model crystals at room temperature even with significant static disorder.[63] All these arguments suggest dominant hopping transport of a highly localized charge carrier in Ph_2-benz-BODIPY crystals at room temperature and the applicability of semiclassical Marcus theory for charge transfer simulations.

6. CONCLUSIONS

On the basis of an extensive investigation of the electronic structure, its fluctuations, and the charge transport of a highly ordered defect-free Ph_2-benz-BODIPY system, we provide insight in the complex interplay between molecular structure, crystal morphology, and their impact on charge transport considering in detail the anisotropy of the charge carrier mobility and the difference between electron and hole transport.

For electron transport, we find that the LUMO couples predominantly to vibrational modes with low and intermediate energy including the central ring. These modes cause an internal reorganization energy for electron transfer λ_- that is more than 50% larger compared to λ_+. The substitution of the hydrogen atoms at the 3,5-position by phenyl rings slightly decreases the value of λ_-. We observe mainly two-dimensional electron transport along the crystal direction with the highest number of nearest neighbors with an average electron mobility of 0.15 $cm^2/(V\ s)$. The corresponding TIs arise from orbital overlap between the phenyl rings and the annulated rings. In summary, we predict that the attachment of the phenyl rings improves the electron transport of Ph_2-benz-BODIPY.

In contrast, the HOMO couples mainly to vibrational modes with strong contributions on both the annulated rings and the phenyl rings. These modes occur mostly at intermediate and high energy. Because of the significant coupling of the HOMO to vibrational modes involving the phenyl rings and an increase in the internal reorganization energy due to the attachment of the substituents at the 3,5-position, we expect that the functionalization is impairing the hole transfer, which is an unintended feature if the material is used as the donor material in a photovoltaic device. However, we obtain a hole mobility of 0.53 $cm^2/(V\ s)$ that clearly exceeds the value obtained for electron transport due to a HOMO−HOMO overlap that is overall better than the LUMO−LUMO overlap and a significantly smaller internal reorganization energy.

In general, we observe that at 300 K the charge transport in the system investigated is strongly limited by the anisotropic crystal structure and bottleneck effects, and thus can be characterized by hopping transport between localized states on molecular dimers. The phenyl functionalization responsible for the specific arrangement in the crystal structure might not be an optimal choice regarding transport since in electronic devices materials with dominant one-dimensional conduction channels exhibit strongly defect-limited charge transport. As other benzannulated aza-BODIPYs show different crystal structures,[10,11] it would be interesting to study in more detail the influence of molecular core functionalization on crystal morphology and the resulting transport anisotropy.

In summary, our investigations can be considered as a starting point for an *in silico* materials design for the class of BODIPY molecules. They will assist in the search for more appropriate NIR absorber materials for OSCs to further improve their efficiency.

■ ASSOCIATED CONTENT

Supporting Information

Details of molecular dynamics simulations, the energetic system parametrization, and additional results. This material is available free of charge via the Internet at http://pubs.acs.org.

■ AUTHOR INFORMATION

Corresponding Author

*E-mail: frank.ortmann@tu-dresden.de, Telephone: +49 (0) 351 46331426.

Notes

The authors declare no competing financial interest.

■ ACKNOWLEDGMENTS

We thank Rafael Gutierrez for critically reading the manuscript and Florian Wölzl for measuring the IR spectrum given in the Supporting Information. We gratefully acknowledge support from the German Excellence Initiative via the Cluster of Excellence EXC 1056 "Center for Advancing Electronics Dresden" (cfAED). Additionally, this work was partially supported by the Heinrich Böll Stiftung, e.V. Computational resources were provided by the Center for Information Services and High Performance Computing (ZIH) of the Dresden University of Technology.

■ ABBREVIATIONS

HOMO, highest occupied molecular orbital; DOS, density of states; IR, infrared; KMC, kinetic Monte Carlo; LUMO, lowest unoccupied molecular orbital; MD, molecular dynamics; MO, molecular orbital; NIR, near-infrared; OSC, organic solar cell; TI, transfer integral

■ REFERENCES

(1) Riede, M.; Lüssem, B.; Leo, K. Organic Semiconductors. *Compr. Semicond. Sci. Technol.* **2011**, *4*, 448−507.

(2) Lungenschmied, C.; Dennler, G.; Neugebauer, H.; Sariciftci, S. N.; Glatthaar, M.; Meyer, T.; Meyer, A. Flexible, Long-Lived, Large-Area, Organic Solar Cells. *Sol. Energy Mater. Sol. Cells* **2008**, *91*, 379−384.

(3) Brédas, J.-L.; Norton, J. E.; Cornil, J.; Coropceanu, V. Molecular Understanding of Organic Solar Cells: The Challenges. *Acc. Chem. Res.* **2009**, *42* (11), 1691−1699.

(4) Riede, M.; Uhrich, C.; Widmer, J.; Timmreck, R.; Wynands, D.; Schwartz, G.; Guehr, W.-M.; Hildebrandt, D.; Weiss, A.; Hwang, J.; et al. Efficient Organic Tandem Solar Cells Based on Small Molecules. *Adv. Funct. Mater.* **2011**, *21*, 3019−3028.

(5) Mueller, T.; Gresser, R.; Leo, K.; Riede, M. Organic Solarcell Based on a Novel Infrared Absorbing Aza-Bodipy Dye. *Sol. Energy Mater. Sol. Cells* **2012**, *99*, 176−181.

(6) Loudet, A.; Burgess, K. BODIPY Dyes and Their Derivatives: Syntheses and Spectroscopic Properties. *Chem. Rev.* **2007**, *107*, 4891−4932.

(7) McDonnell, S. O.; O'Shea, D. F. Near-Infrared Sensing Properties of Dimethlyamino-Substituted BF_2-Azadipyrromethenes. *Org. Lett.* **2006**, *8* (16), 3493−3496.

(8) Zhao, W.; Carreira, E. M. Conformationally Restricted Aza-BODIPY: Highly Fluorescent, Stable Near-Infrared Absorbing Dyes. *Chem.—Eur. J.* **2006**, *12*, 7254−7263.

(9) Gresser, R.; Hartmann, H.; Wrackmeyer, M.; Leo, K.; Riede, M. Synthesis of Thiophene-Substituted Aza-BODIPYs and Their Optical and Electrochemical Properties. *Tetrahedron* **2011**, *67*, 7148−7155.

(10) Gresser, R.; Hummert, M.; Hartmann, H.; Leo, K.; Riede, M. Synthesis and Characterization of Near-Infrared Absorbing Benzannulated Aza-BODIPY Dyes. *Chem.—Eur. J.* **2011**, *17*, 2939−2947.

(11) Donyagina, V. F.; Shimizu, S.; Kobayashi, N.; Lukyanets, E. A. Synthesis of N,N-Difluoroboryl Complexes of 3,30-Diarylazadiisoindolylmethenes. *Tetrahedron Lett.* **2008**, *49*, 6152−6154.
(12) Erten-Ela, S.; Yilmaz, M. D.; Icli, B.; Dede, Y.; Icli, S.; Akkaya, E. U. A Panchromatic Boradiazaindacene (BODIPY) Sensitizer for Dye-Sensitized Solar Cells. *Org. Lett.* **2008**, *10* (15), 3299−3302.
(13) Rousseau, T.; Cravino, A.; Bura, T.; Ulrich, G.; Ziessel, R.; Roncali, J. BODIPY Derivatives as Donor Materials for Bulk Heterojunction Solar Cells. *Chem. Commun.* **2009**, 1673−1675.
(14) Kim, B.; Ma, B.; Donuru, V. R.; Liu, H.; Fréchet, J. M. J. Bodipy-Backboned Polymers as Electron Donor in Bulk Heterojunction Solar Cells. *Chem. Commun.* **2010**, *46*, 4148−4150.
(15) Meiss, J.; Holzmueller, F.; Gresser, R.; Leo, K.; Riede, M. Near-Infrared Absorbing Semitransparent Organic Solar Cells. *Appl. Phys. Lett.* **2011**, *99*, 193307.
(16) Cheng, Y. C.; Silbey, R. J.; da Silva Filho, D. A.; Calbert, J. P.; Cornil, J.; Brédas, J. L. Three-Dimensional Band Structure and Bandlike Mobility in Oligoacene Single Crystals: A Theoretical Investigation. *J. Chem. Phys.* **2003**, *118* (8), 3764−3774.
(17) Ortmann, F.; Bechstedt, F.; Hannewald, K. Charge Transport in Organic Crystals: Interplay of Band Transport, Hopping and Electron-Phonon Scattering. *New J. Phys.* **2010**, *12*, 023011.
(18) Troisi, A.; Orlandi, G. Charge-Transport Regime of Crystalline Organic Semiconductors: Diffusion Limited by Thermal Off-Diagonal Electronic Disorder. *Phys. Rev. Lett.* **2006**, *96* (8), 086601.
(19) Troisi, A. Prediction of the Absolute Charge Mobility of Molecular Semiconductors: the Case of Rubrene. *Adv. Mater.* **2007**, *19*, 2000−2004.
(20) Picon, J.-D.; Bussac, M. N.; Zuppiroli, L. Quantum Coherence and Carriers Mobility in Organic Semiconductors. *Phys. Rev. B* **2007**, *75*, 235106.
(21) Martinelli, N. G.; Olivier, Y.; Athanasopoulos, S.; Delgado, M.-C. R.; Pigg, K. R.; da Silva Filho, D. A.; Sánchez-Carrera, R. S.; Venuti, E.; Della Valle, R. G.; Brédas, J.-L.; Beljonne, D.; et al. Influence of Intermolecular Vibrations on the Electronic Coupling in Organic Semiconductors: The Case of Anthracene and Perfluoropentacene. *Chem. Phys. Chem.* **2009**, *10*, 2265−2273.
(22) Marcus, R. A. Electron Transfer Reactions in Chemistry. Theory and Experiment. *Rev. Mod. Phys.* **1993**, *65* (3), 599−610.
(23) Hutchison, G. R.; Ratner, M. A.; Marks, T. J. Hopping Transport in Conductive Heterocyclic Oligomers: Reorganization Energies and Substituent Effects. *J. Am. Chem. Soc.* **2005**, *127*, 2339−2350.
(24) Schrader, M.; Fitzner, R.; Hein, M. P.; Elschner, C.; Baumeier, B.; Leo, K.; Riede, M.; Bäuerle, P.; Andrienko, D. Comparative Study of Microscopic Charge Dynamics in Crystalline Acceptor-Substituted Oligothiophenes. *J. Am. Chem. Soc.* **2012**, *134*, 6052−6056.
(25) Zhugayevych, A.; Postupna, O.; Bakus, R. C.; Welch, G. C.; Bazan, G. C.; Tretiak, S. Ab Initio Study of a Molecular Crystal for Photovoltaics: Light Absorption, Exciton and Charge Carrier Transport. *J. Phys. Chem. C* **2013**, *117*, 4920−4930.
(26) VandeVondele, J.; Krack, M.; Mohamed, F.; Parrinello, M.; Chassaing, T.; Hutter, J. QUICKSTEP: Fast and Accurate Density Functional Calculations Using a Mixed Gaussian and Plane Waves Approach. *Comput. Phys. Commun.* **2005**, *167*, 103−128.
(27) Krack, M.; Parrinello, M. High Performance Computing in Chemistry. *NIC Ser.* **2004**, *25*, 29−51.
(28) Goedecker, S.; Teter, M.; Hutter, J. Separable Dual-Space Gaussian Pseudopotentials. *Phys. Rev. B* **1996**, *54* (3), 1703−1710.
(29) Hartwigsen, C.; Goedecker, S.; Hutter, J. Relativistic Separable Dual-Space Gaussian Pseudopotentials from H to Rn. *Phys. Rev. B* **1998**, *58* (7), 3641−3662.
(30) Krack, M. Pseudopotentials for H to Kr Optimized for Gradient-Corrected Exchange-Correlation Functionals. *Theor. Chem. Acc.* **2005**, *114*, 145−152.
(31) VandeVondele, J.; Hutter, J. Gaussian Basis Sets for Accurate Calculations on Molecular Systems in Gas and Condensed Phases. *J. Chem. Phys.* **2007**, *127*, 114105.
(32) Becke, A. D. A. New Mixing of Hartree−Fock and Local Densityfunctional Theories. *J. Chem. Phys.* **1993**, *98* (2), 1372−1377.
(33) Becke, A. D. Density-Functional Exchange-Energy Approximation with Correct Asymptotic Behavior. *Phys. Rev. A* **1988**, *38* (6), 3098−3100.
(34) Becke, A. D. Densityfunctional Thermochemistry. III. The Role of Exact Exchange. *J. Chem. Phys.* **1993**, *98* (7), 5648−5652.
(35) Krishnan, R.; Binkley, J. S.; Seeger, R.; Pople, J. A. Selfconsistent Molecular Orbital Methods. XX. A Basis Set for Correlated Wave Functions. *J. Chem. Phys.* **1980**, *72* (1), 650−654.
(36) Frisch, M. J.; Jaramillo, J.; Gomperts, R.; Stratmann, R. E.; Yazyev, O.; Austin, A. J.; Cammi, R.; Pomelli, C.; Ochterski, J. W.; Ayala, P. Y. et al. *Gaussian 03, Revision C.02*; Gaussian, Inc.: Wallingford, CT, 2004.
(37) Novikov, S. V. Organic Glasses: Cluster Structure of the Random Energy Landscape. *Ann. Phys.* **2009**, *18* (12), 949−953.
(38) Coropceanu, V.; Cornil, J.; da Silva Filho, D. A.; Olivier, Y.; Silbey, R.; Brédas, J.-L. Charge Transport in Organic Semiconductors. *Chem. Rev.* **2007**, *107*, 926−952.
(39) Gisslén, L.; Scholz, R. Crystallochromy of Perylene Pigments: Interference between Frenkel Excitons and Charge-Transfer States. *Phys. Rev. B* **2009**, *80*, 115309.
(40) Scott, A. P.; Radom, L. Harmonic Vibrational Frequencies: An Evaluation of Hartree-Fock, Møller-Plesset, Quadratic Configuration Interaction, Density Functional Theory, and Semiempirical Scale Factors. *J. Phys. Chem.* **1996**, *100*, 16502−16513.
(41) Pecchia, A.; Gheorghe, M.; Di Carlo, A.; Lugli, P.; Niehaus, T. A.; Frauenheim, Th.; Scholz, R. Role of Thermal Vibrations in Molecular Wire Conduction. *Phys. Rev. B* **2003**, *68*, 235321.
(42) Russell, G. A.; Klick, C. C. Configuration Coordinate Curves for F-Centers in Alkali Habde Crystals. *Phys. Rev.* **1956**, *101* (5), 1473−1479.
(43) Scholz, R.; Vragovicc, I.; Kobitski, A. Yu.; Salvan, G.; Kampen, T. U.; Schreiber, M.; Zahn, D. R. T. Spectroscopic Properties of a Prototypic Organic Semiconductor: The Case of PTCDA. *Proceedings of International School of Physics "E. Fermi", course CXLIX: Organic nanostructures: Science and applications*; Agranovich, V. M., La Rocca, G. C., Eds.; IOS Press: Amsterdam, 2002; pp 379−403.
(44) Scholz, R.; Schreiber, M. Linear Optical Properties of Perylene-based Chromophores. *Chem. Phys.* **2006**, *325*, 9−21.
(45) Schönherr, G.; Bässler, H. Dispersive Hopping Transport via Sites Having a Gaussian Distribution of Energies. *Philos. Mag. B* **1981**, *44* (1), 47−61.
(46) Borsenberger, P. M.; Pautmeier, L.; Bässler, H. Charge Transport in Disordered Molecular Solids. *J. Chem. Phys.* **1991**, *94* (8), 5447−5454.
(47) Poelking, C.; Cho, E.; Malafeev, A.; Ivanov, V.; Kremer, K.; Risko, C.; Brédas, J.-L.; Andrienko, D. Characterization of Charge-Carrier Transport in Semicrystalline Polymers: Electronic Couplings Site Energies and Charge-Carrier Dynamics in Poly(bithiophene-alt-thienothiophene) [PBTTT]. *J. Phys. Chem. C* **2013**, *117*, 1633−1640.
(48) May, F.; Al-Helwi, M.; Baumeier, B.; Kowalsky, W.; Fuchs, E.; Lennartz, C.; Andrienko, D. Design Rules for Charge-Transport Efficient Host Materials for Phosphorescent OLEDs. *J. Am. Chem. Soc.* **2012**, *134*, 13818−13822.
(49) da Silva Filho, D. A.; Kim, E.-G.; Brédas, J.-L. Transport Properties in the Rubrene Crystal: Electronic Coupling and Vibrational Reorganization Energy. *Adv. Mater.* **2005**, *17* (8), 1072−1076.
(50) Anger, F.; Scholz, R.; Adamski, E.; Broch, K.; Gerlach, A.; Sakamoto, Y.; Suzuki, T.; Schreiber, F. Optical Properties of Fully and Partially Fluorinated Rubrene in Films and Solution. *Appl. Phys. Lett.* **2013**, *102*, 013308.
(51) Scholz, R.; Gisslén, L.; Himcinschi, C.; Vragovic, I.; Calzado, E. M.; Louis, E.; San Fabián Maroto, E.; Díaz-García, M. A. Asymmetry between Absorption and Photoluminescence Line Shapes of TPD: Spectroscopic Fingerprint of the Twisted Biphenyl Core. *J. Phys. Chem. A* **2009**, *113*, 315−324.
(52) Geng, H.; Niu, Y.; Peng, Q.; Shuai, Z.; Coropceanu, V.; Brédas, J.-L. Theoretical Study of Substitution Effects on Molecular

Reorganization Energy in Organic Semiconductors. *J. Chem. Phy.* **2011**, *135*, 104703.
(53) Kresse, G.; Furthmüller, J. Efficiency of Ab-Initio Total Energy Calculations for Metals and Semiconductors Using a Plane-Wave Basis Set. *Comput. Mater. Sci.* **1996**, *6*, 15−50.
(54) Kresse, G.; Furthmüller, J. Efficient Iterative Schemes for Ab Initio Total-Energy Calculations Using a Plane-Wave Basis Set. *Phys. Rev. B* **1996**, *54*, 11169−11186.
(55) Monkhorst, H. J.; Pack, J. D. Special Points for Brillouin-Zone Integrations. *Phys. Rev. B* **1976**, *13*, 5188−5192.
(56) Kohn, W.; Sham, L. J. Self-Consistent Equations Including Exchange and Correlation Effects. *Phys. Rev.* **1965**, *140*, A1133−A1138.
(57) Perdew, J. P.; Zunger, A. Self-Interaction Correction to Density-Functional Approximations for Many-Electron Systems. *Phys. Rev. B* **1981**, *23*, 5048−5079.
(58) Ortmann, F.; Hannewald, K.; Bechstedt, F. Ab Initio Studies of Structural, Vibrational, and Electronic Properties of Durene Crystals and Molecules. *Phys. Rev. B* **2007**, *75*, 195219.
(59) Gollub, C.; Avdoshenko, S.; Gutierrez, R.; Berlin, Y.; Cuniberti, G. Charge Migration in Organic Materials: Can Propagating Charges Affect the Key Physical Quantities Controlling Their Motion? *Isr. J. Chem.* **2012**, *52* (5), 452−460.
(60) Unge, M.; Stafström, S. Effect of Long-Range Correlation on the Metal-Insulator Transition in a Disordered Molecular Crystal. *Phys. Rev. B* **2006**, *74*, 235403.
(61) Picon, J.-D.; Bussac, M. N.; Zuppiroli, L. Quantum Coherence and Carriers Mobility in Organic Semiconductors. *Phys. Rev. B* **2007**, *75*, 235106.
(62) Troisi, A. Dynamic Disorder in Molecular Semiconductors: Charge Transport in Two Dimensions. *J. Chem. Phys.* **2011**, *134*, 034702.
(63) Ortmann, F.; Roche, S. Polaron Transport in Organic Crystals: Temperature Tuning of Disorder Effects. *Phys. Rev. B* **2011**, *84*, 180302.